catalysts

MDPI

Article

Properties of Iron-Modified-by-Silver Supported on Mordenite as Catalysts for NOx Reduction

Perla Sánchez-López [1],*, **Yulia Kotolevich** [1], **Evgeny Khramov** [2],
Ramesh Kumar Chowdari [1], **Miguel Angel Estrada** [1], **Gloria Berlier** [3], **Yan Zubavichus** [4],
Sergio Fuentes [1], **Vitalii Petranovskii** [1] **and Fernando Chávez-Rivas** [5]

[1] Centro de Nanociencias y Nanotecnología, Universidad Nacional Autónoma de México,
    Ensenada 22860, Mexico; julia.kotolevich@gmail.com (Y.K.); chowdarirameshkumar@gmail.com (R.K.C.);
    mestrada@cnyn.unam.mx (M.A.E.); fuentes@ens.cnyn.unam.mx (S.F.); vitalii@cnyn.unam.mx (V.P.)
[2] National Research Center "Kurchatov Institute", Moscow 123182, Russia; evxramov@gmail.com
[3] Dipartimento di Chimica and NIS Centre, Università di Torino, Via P. Giuria 7, 10125 Torino, Italy;
    gloria.berlier@unito.it
[4] Boreskov Institute of Catalysis, Siberian Branch, Russian Academy of Sciences, Novosibirsk 630090, Russia;
    yzubav@gmail.com
[5] Escuela Superior de Física y Matemáticas, Instituto Politécnico Nacional, México City 07738, Mexico;
    fchavezrivas5@gmail.com
* Correspondence: perlaroe@cnyn.unam.mx; Tel.: +52-646-175-0650

check for updates

Abstract: A series of mono and bimetallic catalysts based on a Fe-Ag mixture deposited on mordenite was prepared by ion-exchange and evaluated in the catalytic activity test of the de-NOx reaction in the presence of CO/C_3H_6. The activity results showed that the most active samples were the Fe-containing ones, and at high temperatures, a co-promoter effect of Ag on the activity of Fe catalysts was also observed. The influence of the order of cation deposition on catalysts formation and their physicochemical properties was studied by FTIR (Fourier Transform Infrared Spectroscopy) of adsorbed NO, XANES (X-ray Absorption Near-Edge Structure), and EXAFS (Extended X-ray Absorption Fine Structure) and discussed in terms of the state of iron. Results of Fe K-edge XANES oscillations showed that, in FeMOR catalysts, iron was present in a disordered state as Fe^{3+} and Fe^{2+}. In FeAgMOR, the prevailing species was Fe^{3+}, while in the AgFeMOR catalyst, the state of iron was intermediate or mixed between FeMOR and FeAgMOR. The Fe K-edge EXAFS results were characteristic of a disordered phase, the first coordination sphere being asymmetric with two different Fe-O distances. In FeAgMOR and AgFeMOR, coordination of Fe-O was similar to Fe_2O_3 with a few amount of Fe^{2+} species. We may conclude that, in the bimetallic FeAgMOR and AgFeMOR samples, a certain amount of tetrahedral Al^{3+} ions in the mordenite framework is replaced by Fe^{3+} ions, confirming the previous reports that these species are active sites for the de-NOx reaction. Based on the thermodynamic analysis and experimental data, also, it was confirmed that the order of deposition of the components influenced the mechanism of active sites' formation during the two steps ion-exchange synthesis.

Keywords: iron; silver; mordenite; bimetallic; deposition order; ion exchange; de-NOx

1. Introduction

Reducing NOx emissions (de-NOx) is an important problem facing modern technology. NOx plays a critical role in air pollution and in the physicochemical processes in the troposphere due to its chemical activity in the environment, which causes photochemical smog and acid rain [1,2]. Moreover, the role of NOx emissions in global warming is also of paramount importance [3] since N_2O has an absorption

efficiency for trapping heat 200–300 times greater than CO_2. One of the main sources of NO_x emissions is vehicles powered by internal combustion engines, and in particular, diesel engines [4]. Even in the presence of increasingly stricter regulations, control of NO_x emissions in automotive remains yet to be fully resolved by the responsible agencies of each country and by the scientific community [5–8]. Consequently, excess NO_x emissions continue to be a serious environmental problem, as well as the toxic effects they cause on living beings [9,10]. In order to reduce NO_x emissions, the selective catalytic reduction of NO_x with hydrocarbons (HC-SCR) using transition metal exchanged zeolites has been extensively studied over the last two decades [11–15]. However, this method still requires important improvements, as well as the development of more efficient, active, stable, and selective catalysts.

Understanding the processes of the formation of active forms is an important step towards creating the most effective catalyst. The reported research and characterization of de-NO_x catalysts are focused mainly on the identification of the active sites and their interaction with the support [16–18]. The most active systems being studied are based on transition metals (mainly group IB and VIIIB of the periodic table) [19–22] and their multimetallic mixtures [23–25] because they show good catalytic performance. The transition metals are mainly supported on zeolites, such as MOR (Mordenite) [26], BEA (Beta) [27], MFI (Zeolite Socony Mobil-five or ZSM-5) [28], FER (Ferrierite) [17], and CHA (Chabazite) [29], because of their thermal stability, high availability of acid sites, and their catalytic performance in de-NO_x processes. Mordenite zeolite, in particular, has important structural characteristics that provide a good catalytic performance in HC-SCR of NO_x owing to its medium pore size, high surface area, high availability of exchange sites, and stable framework. Besides, mordenite possesses properties, such as water tolerance [30], high adsorption capacity [31], and the potential for clusters stabilization [32]. These intrinsic properties make mordenite suitable support for a thermally stable de-NO_x catalyst with controlled acidity.

Recently, catalysts based on silver and iron supported on different substrates have attracted much attention due to their redox properties and wide operation temperature for the de-NO_x removal process [33–35]. The interest in using Fe lies in its high catalytic performance in a wide temperature window (250–450 °C) and redox properties during the NO_x reduction. According to Shi et al. [36], iron catalysts supported on MFI exhibited efficient catalytic performance due to the synergistic effect between isolated Fe^{3+} and Fe_2O_3. Likewise, Dzwigaj et al. [37] studied iron impurities in MOR, BEA, and MFI and their effect on the catalytic activity in SCR of NO_x. Results showed that the Fe^{3+} species in tetrahedral and octahedral coordination were responsible for the catalytic activity in the zeolites studied. Consequently, iron in the 3+ oxidation state is an active site, demonstrating good catalytic performance in NO_x reduction with hydrocarbons, as demonstrated by many researchers [38–43]. The silver-based catalysts evaluated in HC-SCR of NO_x have shown acceptable catalytic performance at low temperatures (below 300 °C), which has been associated with different silver species (cations, nanoparticles, and clusters). Bartolomeu et al. [16,44] studied the silver species associated with catalytic activity in NO_x reduction. They found that the activity of silver catalysts was mainly due to Ag^+ ions, Ag_m^{n+} clusters, and Ag^0 nanoparticles formed by redox cycles. The same has been observed by other authors [45–47]. Therefore, Ag has been studied as a promoter in de-NO_x catalysts to increase the operating temperature range [48]. Although Ag is well known as an iron modifier, their interaction can affect structural, adsorptive, electronic, redox, and catalytic properties in various reactions. Given the individual catalytic properties of silver and iron, the interaction between these metals allows us to develop more efficient catalytic centers for the de-NO_x reaction in order to achieve high NO_x conversions.

The order of deposition of the metal components in the preparation of bimetallic catalysts has been shown to strongly influence the redox interaction of metals, contributing to the formation of sites of interest for HC-SCR of NO_x [49,50]. Based on these premises, the goal of this work was to study the formation of Fe-Ag species deposited on mordenite and their physicochemical properties, focusing on a two steps ion-exchange procedure with a different order of insertion. The catalytic properties of the studied materials were tested for the environmentally important reaction of de-NO_x by HC-SCR.

2. Results and Discussion

Mordenite is a medium pore size zeolite, where the negative charge induced by the presence of aluminum in the neutral silicate framework needs to be compensated by cations. Charge compensating exchangeable cations are located in the zeolite channels and pores. The sum of the charges of all counterions divided by the aluminum content (called the equilibrium ion-exchange modulus (EIEM)) should be equal to 1. In this study, the cations used are Ag^+, Fe^{2+}, Fe^{3+}, and H^+ (from the acidified iron precursor solution), along with residual Na^+ of the initial mordenite (if any):

$$\text{EIEM} = \frac{1\left[Na^+\right] + 1\left[Ag^+\right] + 1\left[H^+\right] + 2\left[Fe^{2+}\right] + 3\left[Fe^{3+}\right]}{[Al]} = 1, \tag{1}$$

We have to underline that the EIEM calculations based on the integral concentration of the components are complicated due the presence of some amount of reduced Ag^0, which are forming clusters and nanoparticles, as well as the dual role of Fe, which partially balances the charge of Al-containing tetrahedra, but also partially substitutes Al in tetrahedral coordination, and also needs to be equilibrated by some extra lattice cations.

The chemical composition of the samples, as measured by ICP-OES (Inductively Coupled Plasma-Optical Emission Spectroscopy), is presented in Table 1. By comparing the Si/Al ratio of monometallic and bimetallic samples with the original value for the NaMOR, it can be seen that all samples, except AgMOR, have presented a weak dealumination, which is attributed to the acidic pH of the iron-containing solution.

Table 1. Chemical composition of the samples, measured by Inductively Coupled Plasma-Optical Emission Spectroscopy (ICP-OES).

Sample	Atomic, %								
	Si	Al	O	Ag	Fe	Na	Si/Al	EIEM	
								EIEM–Fe^{2+}	EIEM–Fe^{3+}
NaMOR	48.9	7.5	33.9	-	-	9.7	6.5	1.29	
AgMOR	38.1	5.8	49.9	4.6	-	1.6	6.5	1.07	
FeMOR	44.0	6.4	45.4	-	0.8	3.4	6.8	0.78	0.91
FeAgMOR	37.2	5.4	51.9	3.6	0.4	1.5	6.9	1.09	1.17
AgFeMOR	39.7	5.9	49.7	3.1	0.9	0.7	6.7	0.95	1.10

The EIEM is calculated from the ICP-OES results for all samples (see Table 1). Different values are observed between NaMOR, AgMOR, and Fe-containing samples. Since it is impossible to estimate the number of iron cations those who enter in the framework and evaluate the ratio between the coexisting Fe^{2+} and Fe^{3+} cations [50] from the ICP-OES data, the limit values of EIEM-Fe^{2+} and EIEM-Fe^{3+} are calculated, considering that all the iron is entirely as cations of one of the possible oxidation states (Fe^{2+} or Fe^{3+}). The real EIEM for our samples should approximate to an intermediate value between the two calculated idealized estimations:

$$\text{EIEM} - Fe^{2+} = \frac{1\left[Na^+\right] + 1\left[Ag^+\right] + 1\left[H^+\right] + 2\left[Fe^{2+}\right]}{[Al]}, \tag{2}$$

$$\text{EIEM} - Fe^{3+} = \frac{1\left[Na^+\right] + 1\left[Ag^+\right] + 1\left[H^+\right] + 3\left[Fe^{3+}\right]}{[Al]}, \tag{3}$$

For most samples, EIEM is close to 1, with the exception of NaMOR and FeMOR. The high EIEM value for NaMOR has been previously associated with the fact that NaOH, which is present during the synthesis of zeolite in the industrial process, is not completely removed by washing of the resulting material [50]. For FeMOR, the EIEM has a value of less than 1. This can be explained by the

participation of H^+ in the process of ion exchange. Since it is not possible to evaluate the amount of H^+ by ICP-OES, therefore, its content is not considered in the EIEM calculations.

It is also seen that despite the same nominal relative concentration per unit charge of both solutions of Ag^+ and Fe^{2+} precursors, the ion exchange of sodium for iron in FeMOR is significantly lower than for silver in AgMOR. In addition, a lower Fe content is observed compared to Ag in both bimetallic samples. This can be explained by the difference in the selectivity of the exchange of Na^+ ions for Ag^+ and Fe^{2+} cations. The second step of ion exchange during the preparation of bimetallic samples do not have a significant effect on the sodium content but decreases the content of the first exchangeable cation; that is, the second stage of exchange occurs due to the leaching of cations that entered in mordenite during the first stage of the exchange.

In multimetallic materials based on zeolites, cation competition for ion exchange sites can take place. The difference in the adsorption capacity of zeolites for heavy metal ions may be attributed to several factors, including hydrated ion diameters, hydration enthalpies, charge-to-radius (Z/r) ratio, and cation solubility, as discussed by Motsi et al. [51].

In addition to those mentioned above, it has been reported that the adsorption of nickel (II) ions on Na-mordenite depends on pH [52]. Both Zn^{2+} [53] and Co^{2+} [54] exhibit practically the same behavior on different zeolites. Nakamura et al. [55] listed the requirements that determine the adsorption capacity of zeolites:

- The radius of micropores must be comparable to the ionic radius of the target cation.
- The Si/Al ratio should not be very high; moderate ratios are preferred; in such case, the zeolite framework becomes more negatively charged, and then the cation adsorption capacity is enhanced.
- A uniform distribution of ion-exchange centers (i.e., Al atoms) around channels and cavities is required [56].

To evaluate the adsorption capacity of mordenite with respect to target cations, we have examined the ratio of charge to radius Z/r, enthalpy of hydration [57], and dissociation energy of cation-oxygen bonds [58] (see Table 2). The enthalpy of hydration is the amount of energy released due to the interaction of one mole of ions with water dipoles and characterizes the solubility of ions. The dissociation energy of the cation-oxygen bond is one of the indicators of the strength of this chemical bond. Thus, the difference between these two energetic contributions can characterize the transition from the state associated with the zeolite to the dissolved state. Based on these theoretical parameters, we might suggest the mechanism of adsorption.

Table 2. Parameters of the target cations.

Target Cation	(Z/r) pm	Cation-oxygen Bond Dissociation Energies, kJ mole^{-1}	Hydration Enthalpy, kJ Mole^{-1}	$-\Delta H^\circ$ of the Transition of the Cation from the Zeolite-Bound State to the Dissolved State, kJ mole^{-1}
Na^+	102	270 ± 4	409 ± 3	139
Ag^+	115	221 ± 21	473 ± 3	252
H^+	10	430 ± 0.29	1091 ± 5	661
Fe^{2+}	78	407 ± 1	1946 ± 6	1539
Fe^{3+}	65	407 ± 1	4430 ± 10	4023

As can be seen from Table 2, for all considered cations, this transition is exothermic. $-\Delta H^\circ$ changes in the sequence: $Na^+ > Ag^+ > H^+ > Fe^{2+} > Fe^{3+}$, which means that all additional cations are able to replace Na^+, which balances the negative charge of the zeolite structure. Thus, based on the data in Table 2, it can be assumed that during the preparation of FeMOR (treatment of NaMOR in a solution containing Fe^{2+} and H^+), Na^+ is exchanged for both H^+ and Fe^{2+}.

This is in good agreement with the ICP-OES data presented in Table 1, where the values of both EIEM-Fe^{2+} and EIEM-Fe^{3+} are below 1, which confirms the presence of H^+ in FeMOR. From Table 2,

it can also be assumed that H^+ can replace Ag^+, also during the synthesis of AgFeMOR (AgMOR treatment in a solution containing Fe^{2+} and H^+, EIEM-Fe^{2+} = 0.95), but Ag^+ could not replace H^+ during the preparation of FeAgMOR. The sequence to form this system is Fe(H^+)MOR in the Ag^+ solution (EIEM-Fe^{2+} = 1.09). Since the EIEM-Fe^{2+} for both bimetallic samples is close to 1, we cannot assume the contribution of H^+ to the second ion-exchange step of the synthesis. According to Table 2, iron ions have the greatest exothermic effect; however, among all the studied cations, these two are multi charged, and their interaction with singly charged Al-tetrahedrons in the zeolite lattice may have steric limitations.

The treatment of FeMOR with an Ag^+ solution mainly leads to the exchange of Na^+ remaining in the sample for Ag^+. At the same time, the contact between Ag^+ and Fe^{2+} on the surface creates a redox interaction, leading to the formation of Ag^0 and Fe^{3+} in MOR. A zero-charged silver atom could not displace Fe^{3+} from its position. Thus, it is expected that a mixture of Ag^0 and Ag^+ species will form in FeAgMOR, with the simultaneous formation of a significant amount of Fe^{3+}. Treatment of AgMOR in the Fe^{2+} plus H^+ solution can lead to the exchange of the Na^+ residue with H^+ and Fe^{2+}. Otherwise, the redox interaction between AgMOR and Fe^{2+} cations causes Ag^0 to leave the negatively charged site. At this point, the vacant negatively charged site [-]MOR may be occupied by oxidized Fe^{3+} or Fe^{2+} or H^+ from the solution. Thus, in the case of AgFeMOR, a large number of Ag^0-species and a mixture of Fe^{2+} and Fe^{3+} are expected. In the future, an attempt will be made to further refine the suggested mechanism for preparing samples with a different order of cation deposition, using additional data from various experimental methods, but such study is beyond the scope of this work and will be published elsewhere.

The textural properties of the samples are listed in Table 3. A comparison of the properties (surface area, pore-volume, and pore diameter) of the synthesized samples with the initial NaMOR indicates that no significant variations have been observed. It can be noted that the FeMOR sample presents a slight increase in the specific surface area, about 60 $m^2 \cdot g^{-1}$, but this is exactly the sample in which there is a significant fraction of ion-exchanged protons (see EIEM value, Table 1), which probably reduces steric hindrances to adsorption.

Table 3. Textural properties of the studied samples.

Sample	S_{BET}, $m^2 \cdot g^{-1}$	V_{total}, $cm^3 \cdot g^{-1}$	V_{micro}, $cm^3 \cdot g^{-1}$	Pore Diameter, Å
NaMOR	338	0.19	0.16	22.8
AgMOR	322	0.19	0.14	23.2
FeMOR	398	0.23	0.17	23.3
AgFeMOR	343	0.20	0.15	23.7
FeAgMOR	336	0.20	0.14	24.1

Qualitative and quantitative analysis of the Brønsted surface acidity of the synthesized materials has been performed by the method of ammonia TPD (Temperature Programmed Desorption) in the range of 100–550 °C, and the data are presented in Table 4. Desorption of ammonia for all the samples is characterized by two main peaks: one at about 180 °C (*l-peak*), which can be correlated with weak acid sites, and another about 250 °C (*h-peak*), which corresponds to strong acid sites. In the case when silver is exchanged at the first stage (AgMOR and AgFeMOR), the ratio of weak/strong acid centers does not change and is in good agreement with the initial data for NaMOR (~30:70). However, when the iron is exchanged the first (FeMOR and FeAgMOR), the mentioned ratio changes significantly: the amount of weak acid sites decreases, and the amount of strong acid sites increases (16:84 and 19:81 for FeMOR and FeAgMOR, respectively).

Table 4. Surface acid sites characterization of studied samples by Temperature Programmed Desorption (TPD) of adsorbed NH_3.

Sample	Amount of the Acid Sites, %		Total Acidity, mmol/g
	l-peak	*h-peak*	
NaMOR	32	68	1359
AgMOR	33	67	1662
FeMOR	16	84	2970
AgFeMOR	29	71	2264
FeAgMOR	19	81	1251

When iron is deposited in the last stage of ion exchange in AgFeMOR, despite maintaining the volume exchange ratio, the total acidity increases significantly due to the presence of protons (from the precursor solution acidified with H_2SO_4). These protons can replace cationic sites, as suggested by ICP-OES data (Table 1) and thermodynamic parameters (Table 2). Thus, the order of deposition of the components affects the surface acidity, which, in turn, affects the catalytic properties.

To estimate the ratio of Fe^{2+} and Fe^{3+} in as-prepared samples, FTIR measurements of adsorbed NO have been performed; the results are shown in Figure 1. Adsorption of NO on the initial mordenite and on AgMOR is negligible, while all Fe-containing samples have shown intense absorption bands corresponding to the nitrosyl complexes of Fe: $Fe^{3+}(NO)$ at 1883 cm^{-1} and $Fe^{2+}(NO)_n$, where n = 1 at 1852 cm^{-1}, n = 2 at 1766 cm^{-1}, n = 3 at 1813 and 1919 cm^{-1} [59]. All Fe-containing samples have the presence of both nitrosyl complexes, based on Fe^{2+} and Fe^{3+}. As mentioned above, the Fe content in FeAgMOR is lower than in the other two Fe-containing samples; accordingly, the intensity of absorption of NO on FeAgMOR is also approximately two times lower.


Figure 1. *Cont.*

(e)
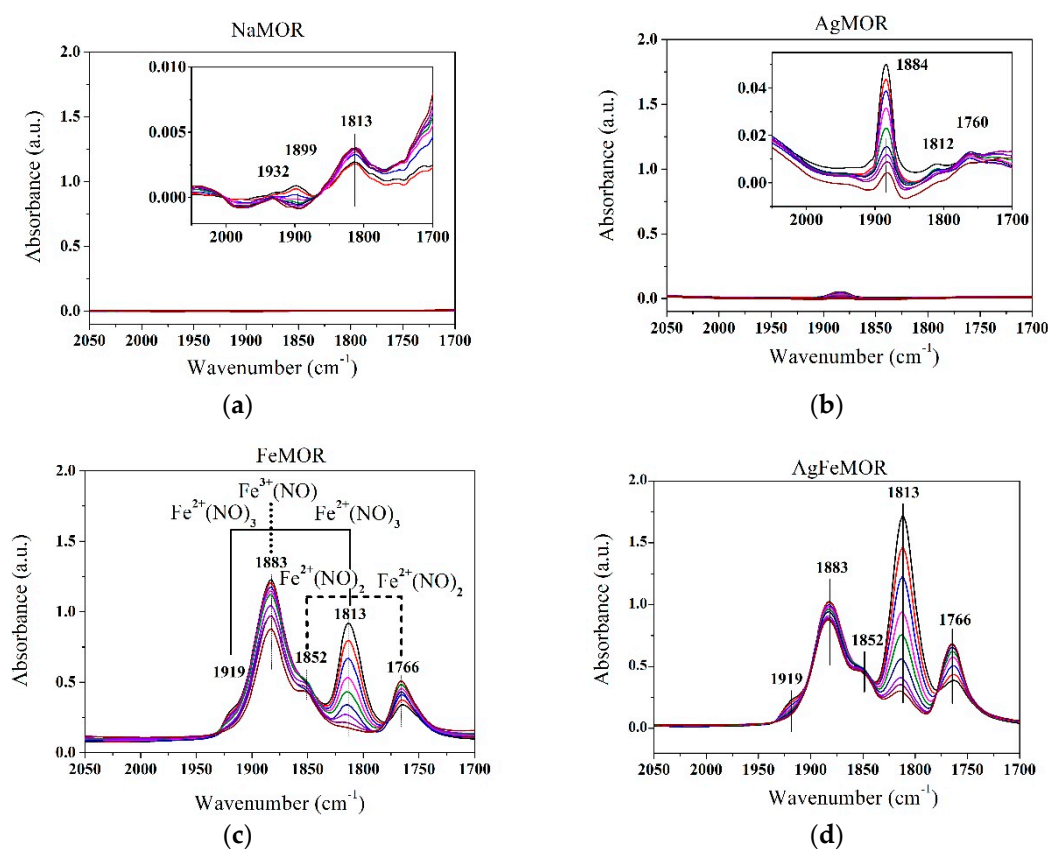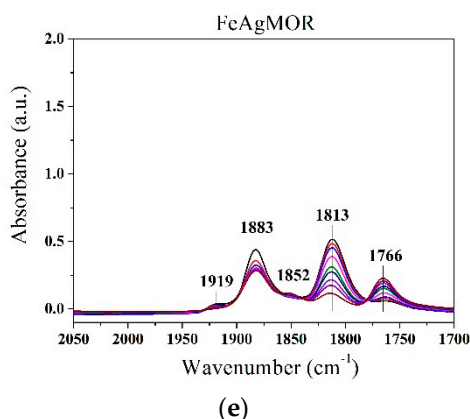
Figure 1. FTIR spectra of adsorbed NO on studied samples. (**a**) NaMOR; (**b**) AgMOR; (**c**) FeMOR; (**d**) AgFeMOR, and (**e**) FeAgMOR. All spectra are normalized with respect to the pellet thickness and reported in the same vertical range for easier comparison. The spectra are measured by dosing NO; the NO pressure is decreased from 70 mBar (black dotted line) to a dynamic vacuum of 5.0×10^{-4} mBar (cherry dotted line). Insets in panels (**a**) and (**b**) report a magnification of the corresponding (very weak) spectra.

As seen from Figure 1c-e, bands of nitrosyl complexes $Fe^{2+}(NO)_n$ with n = 1 and 2 appear first. Then, with an increase of NO pressure, both of them transform into the adsorption band corresponding to $Fe^{2+}(NO)_n$ with n = 3. Complex adsorption band $Fe^{3+}(NO)$ shows a maximum of intensity at an intermediate level of pressure, and then with increasing pressure, the intensity decreases. For AgFeMOR, the $Fe^{2+}(NO)_3$ adsorption band increases significantly with increasing NO pressure, while the intensity of the $Fe^{3+}(NO)$ band remains virtually unchanged. The intensities of the two mentioned bands for FeMOR and FeAgMOR change more or less the same with the increase in pressure. It could mean that the adsorption sites on the surface of AgFeMOR are different from those on FeMOR and FeAgMOR.

The FTIR spectra of NO are measured after thermal treatment under vacuum, which is known as a mildly reducing activation condition for Fe-zeolites. On all Fe-containing samples, NO reveals the co-existence of Fe^{2+} and Fe^{3+}. This does not allow us to quantify the amount of Fe^{2+} and Fe^{3+} ions before thermal treatment but gives an indication of the effect of Ag on the redox properties of iron. Since only one band at 1883 cm^{-1} is due to the Fe^{3+} state, by comparing its intensity for FeMOR and AgFeMOR samples with similar content of Fe, we can conclude that the Fe^{3+}-content in AgFeMOR is higher than in FeMOR. This can be explained by the redox reaction between Ag^+ and Fe^{2+}, as a result of which Ag^0 and Fe^{3+} are formed, and which is present only in bimetallic samples. Besides, the interaction of NO is stronger for Fe-containing samples (compared to AgMOR and NaMOR), which allows one to expect higher catalytic activity in the de-NO_x reaction.

The XANES and EXAFS methods are applied to shed light on the mechanism of species formation from the point of view of the immediate atomic environment of iron. Fe K-edge XANES spectra (Figure 2a) for all Fe-containing samples are similar to the reference α-Fe$_2$O$_3$, indicating that Fe is mostly present in the Fe^{3+} oxidized state. However, compared to the reference, the intensity of oscillations is reduced, especially for FeMOR, which means that the structure is disordered, and, possibly, another oxidized state of Fe (Fe^{2+}) is present. EXAFS Fourier transforms (Figure 2b) have shown that the spectra of FeMOR are closer to the FeO reference, while the shapes of EXAFS Fourier transforms for both bimetallic samples remain partially similar to those of the α-Fe$_2$O$_3$ reference. It could be explained by the redox reaction of Fe^{2+} with Ag^+, leading to the formation of Fe^{3+} [50] and the presence of iron in both oxidation states simultaneously. In the case of AgFeMOR, the free Fe^{2+} present in the solution undergoes a redox reaction with Ag^+MOR, and consequently, the resulting Ag^0 diffuses from the mordenite channels, agglomerating into nanoparticles in the mesopores and on the surface of crystals. Negatively charged vacancies are compensated by Fe^{3+} ions. In the case of FeAgMOR synthesis, free

Ag^+, which is present in excess in the exchange solution, undergoes a redox reaction with $Fe^{2+}MOR$ to form $Fe^{3+}MOR$, and, as a result, Ag^0 is leached out from the mordenite channels, while other Ag^+ ions from the solution balance the negative charge of the framework.
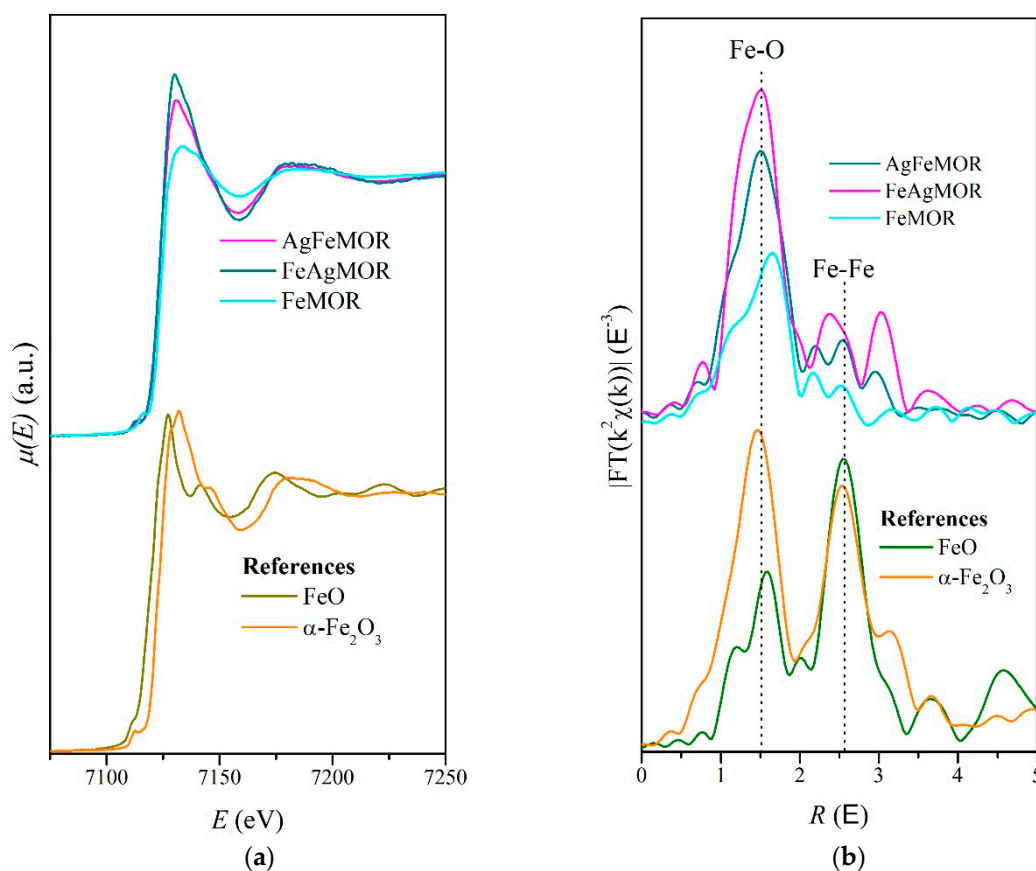
Figure 2. Fe K-edge XANES-spectra (normalized X-ray absorption spectra). (**a**) X-ray Absorption Near-Edge Structure (EXAFS) pattern and (**b**) Fourier transforms taken in the k-range of 2 to 12 Å^{-1}.

Similar to XANES, Fe K-edge EXAFS (Figure 2b) demonstrates that iron in MOR is oxidized. The main maximum of EXAFS Fourier transforms for all MOR samples is very similar to Fe-O maximum for oxide references and, therefore, corresponds to the oxygen surroundings of Fe. However, this Fe-O maximum tends to be asymmetric. To account for this asymmetry, the range of Fourier transforms from 1.2 to 2.1 Å is modeled with two different Fe-O distances; the obtained parameters are shown in Table 5. The fit results suggest that in FeAgMOR and AgFeMOR catalysts, the coordination of Fe-O is similar; for both samples, the coordination numbers are 2+2 (two O atoms each, at two different distances), with Fe-O distances of ~1.9 and ~2.1 Å. Despite the fact that XANES data are similar to the reference α-Fe_2O_3 for these samples, the coordination of Fe in α-Fe_2O_3 is different (octahedral, i.e., 4+2). Moreover, for iron in Fe-containing samples, the maxima, which corresponds to the outer coordination spheres (Fe-Fe, as it is shown in Figure 2a), is either weak or absent. Therefore, based on the EXAFS data, we may conclude that Fe in FeAgMOR and AgFeMOR is partially included in the zeolite framework as Fe^{3+} instead of Al^{3+}. Previously, the mechanism of the isomorphous substitution of Al^{3+} in the mordenite framework by tetrahedrally coordinated Fe^{3+}, which is promoted by the presence of Ag^+ ions, has been proposed and confirmed by Mössbauer spectroscopy, and it has also been shown that the presence and concentration of the framework Fe^{3+} ion in various samples correlate with their catalytic activity in de-NO$_x$ [33].

**Table 5.** Structural parameters obtained from Fe K-edge EXAFS fitting (R-range 1.2 to 2.1 Å, k-range 2 to 12 Å^{-1}, kw = 3).

Sample	Scattering Path	Coordination Number	Interatomic Distance, Å	Debye Factor, Å^2	R-Factor, %
FeMOR	Fe-O	0.6 1.9	1.85 2.06	0.0061 0.0061	1.7
AgFeMOR	Fe-O	1.6 2.0	1.94 2.10	0.0049 0.0049	0.9
FeAgMOR	Fe-O	2.0 2.2	1.91 2.07	0.0024 0.0024	1.9

In the FeMOR sample, the coordination numbers are even lower, 0.6+2, which, along with a decrease in the intensity of XANES oscillations, indicates a disordered or mixed state of Fe, which is different from the states of Fe in bimetallic samples. Taking into account the reduced values of coordination numbers, we assume that this state may include other oxidized states of Fe (i.e., Fe^{2+}). The coordination of Fe in FeAgMOR and FeMOR is different, while AgFeMOR demonstrates intermediate coordination between them. Besides, the intensity of XANES oscillations in AgFeMOR is also slightly decreased compared to the α-Fe_2O_3 reference, which means that, in this sample, the state is intermediate or mixed between FeMOR (disordered state of both Fe^{3+} and Fe^{2+}) and FeAgMOR (dominated by Fe^{3+}).

The samples are tested in the de-NO_x reaction in the presence of a CO/C_3H_6 mixture, after oxidation in a flow of a mixture of oxidants (4.4 vol.% of O_2/N_2 balanced) at a heating rate of 5 °C/min from room temperature up to 550 °C. The catalytic evaluation results are presented in Figure 3. Mordenite itself has shown catalytic activity with a maximum at 312 °C that is attributed to the active sites of the Na^+ cation that acts as a Lewis acid site, while the oxygen framework with partial negative charge acts as a Lewis base. The AgMOR catalyst presents low-temperature activity (120–150 °C), which is associated with the Ag^+, and two peaks at 260 and 377 °C. The latter has shown an increased conversion at temperatures in the range of 320–520 °C, which could be due to the reduction of $Ag^+\rightarrow Ag^0$ under the reaction conditions.
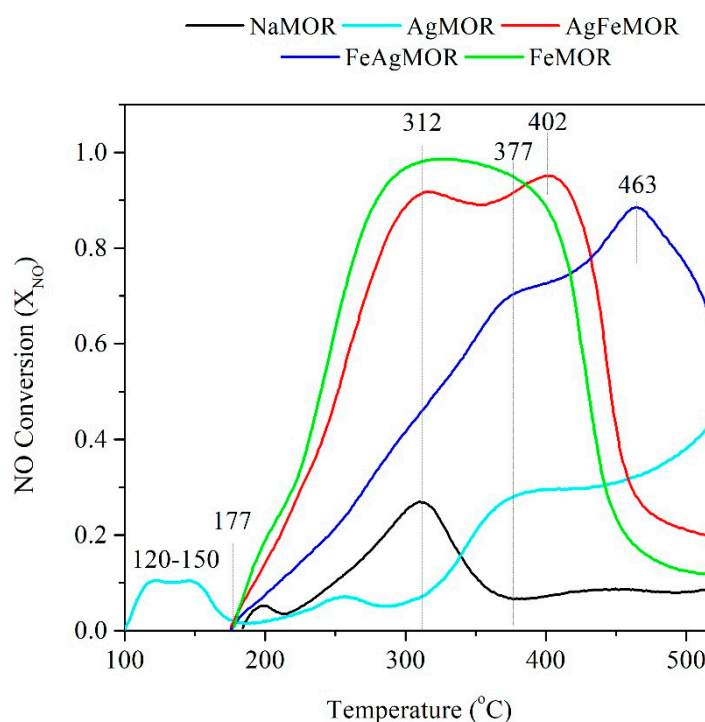
**Figure 3.** Results of the de-NO_x catalytic test for the studied samples.

Since all samples are subjected to preliminary oxidative treatment, the observed activity should be attributed to the oxidized states of the active components (Fe^{3+} and Ag^+) present in the catalyst. However, as it has been confirmed by EXAFS (see above) for AgFeMOR and FeAgMOR catalysts, the presence of Fe^{3+} species is possible in two forms: as a compensation cation on a vacant negatively charged site of mordenite or in the mordenite framework instead of Al^{3+}. The FeMOR catalyst shows ~100% conversion of NO in the range 290–380 °C, and it contains only Fe^{3+} in the ion-exchange sites of mordenite, which are active centers for the de-NO_x.

AgFeMOR shows at least two types of active centers with pronounced maxima at 312 and 402 °C. Those centers, which are active at 312 °C, may be related to Fe^{3+} species interacting with NaMOR since FeMOR shows activity at the same temperature. The active center at about 402 °C can be related to Ag^0 centers, similar to those of the AgMOR sample; however, the activity of these centers on the AgFeMOR is much higher than the ones on the monometallic AgMOR. This can be explained by the activity of Ag^0 formed by the redox interaction of Ag^+ with Fe^{2+} during preparation and by the reduction of Ag^+ residue under the reaction conditions. Two types of active centers represent the operating temperature window for the conversion of NO over FeAgMOR: the peaks at 312 and 463 °C correspond to Fe and Ag species, respectively. Since the Fe content in FeAgMOR is half that in FeMOR and AgFeMOR in accordance with the ICP-OES results, the FeAgMOR activity at 312 °C is lower. Activity after 350 °C of FeAgMOR has a complex temperature correlation, most likely due to the co-existence of different active centers.

According to the de-NO_x, XANES, and EXAFS data, and our previous results [33], the de-NO_x activity can be provided by two types of active centers: Fe^{3+} compensating cation at the vacant negatively charged site of mordenite, or Fe^{3+} in the mordenite framework instead of Al^{3+}. Due to the complex correlation of activity with temperature, until now, it has not been possible to determine a reliable difference between them. The most promising catalysts for the de-NO_x reaction in the presence of CO/C_3H_6 are FeMOR and AgFeMOR. These two samples also have the highest total acidity. The activity profiles of the two mentioned samples are close to each other, which allows us to conclude that silver does not improve the catalytic properties of Fe by itself. However, Ag provides the effect of modifying the catalytic activity of Fe at high temperatures (after 350 °C) by changing the structure of the active centers of iron.

Thus, the experimental results confirm the differences in the mechanism of formation of diverse active species with different orders of cation deposition, proposed on the basis of theoretical parameters (see Table 2). According to EXAFS and NO adsorbed FTIR data for a monometallic FeMOR sample, it has been shown that the most common species are in the Fe^{2+} state (Scheme 1, Step 1A). Treatment of FeMOR with an Ag^+ solution results in the replacement of Na^+ by Ag^+ (Scheme 1, Step 2A). Contact between Ag^+ and Fe^{2+} leads to a redox interaction, resulting in the formation of Ag^0 and Fe^{3+}MOR. A neutrally charged silver atom is unable to displace Fe^{3+} from its position. Thus, the FeAgMOR is expected to have a mixture of Ag^0 and Ag^+ species, while Fe^{3+} is the predominant state of iron. Moreover, for bimetallic samples, it has been confirmed by EXAFS that Fe^{3+} is partially incorporated into the framework of the mordenite.

When AgMOR is treated with Fe^{2+} solution containing H^+ protons, residual Na^+ can be exchanged with both H^+ and Fe^{2+} (Scheme 1, Step 2B). However, the redox interaction between AgMOR and Fe^{2+} leads to the fact that the reduced neutral Ag^0 leaves the negatively charged site. Simultaneously, the vacant negatively charged site [-]MOR can be occupied by oxidized Fe^{3+}, or either Fe^{2+} or H^+ from solution. Thus, in the case of AgFeMOR, it is expected that it will contain a large number of Ag^0-species and a mixture of Fe^{2+} and Fe^{3+}, plus Fe^{3+} embedded into the framework of the mordenite, which is confirmed by the EXAFS data. The results obtained allow us to outline the next step of this study, which will be the study of the formation and state of silver in these samples, which will additionally confirm the presented mechanism. The received data will be published elsewhere.
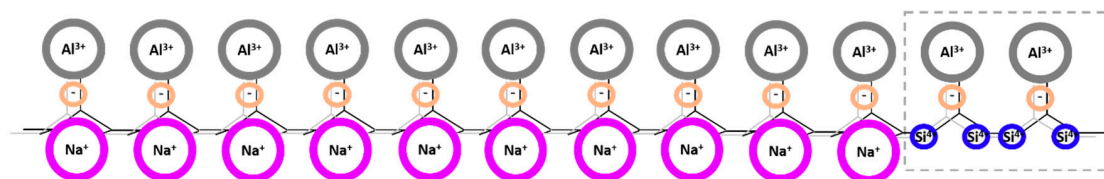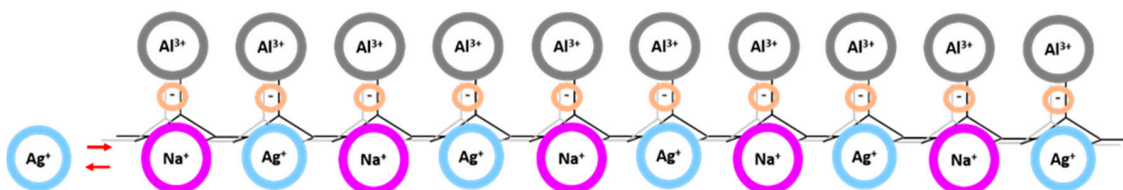
Step 0. Original NaMOR zeolite. The Si atoms in NaMOR are omitted for clarity of mechanism (highlighted in navy blue).
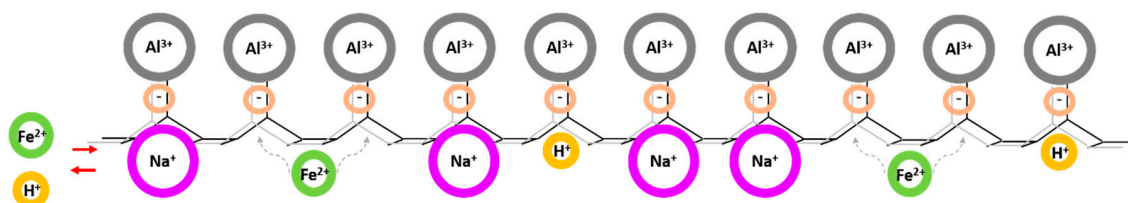
Step 1A. Formation of FeMOR.
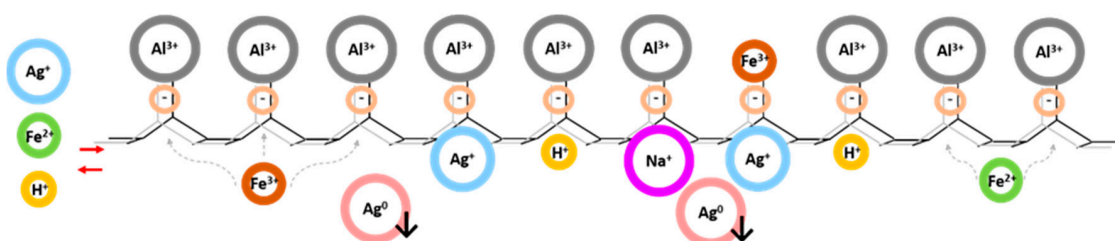
Step 2A. Formation of FeAgMOR.

Step 1B. Formation of AgMOR.

Step 2B. Formation of AgFeMOR.

Scheme 1. Mechanism of the formation of the studied samples during the ion exchange process with a different order of incorporation.

3. Materials and Methods

3.1. Samples Preparation

The sodium form of mordenite (NaMOR) with an atomic ratio Si/Al = 6.5 was supplied by Zeolyst Int. (Product CBV10A, Conshohocken, PA, USA) and was used without any pretreatment/purification. Metals (Ag, Fe) were introduced into the starting mordenite by the conventional ion exchange method from solutions for 24 h at 60 °C, in a ratio of 1 g of NaMOR per 35 mL of the precursor solution.

The precursor of Ag was an aqueous solution of $AgNO_3$ (0.03 N). The Fe precursor was an aqueous solution of $FeSO_4$ (0.03 N), stabilized from hydrolysis by the addition of H_2SO_4 until pH = 2 was adjusted; this value was chosen in accordance with the data [60]. After each ion exchange procedure, the samples were filtered, washed, and dried at 110 °C for 20 h. For the preparation of bimetallic samples, the obtained monometallic samples were processed under similar conditions in appropriate solutions. All ion exchange steps were carried out under conditions that prevent direct light from entering the samples and reducing the illumination time to a minimum in order to avoid the potential reduction of silver ions under the action of light.

For each sample preparation, 2 g of NaMOR was processed using solutions containing the same total metal equivalent concentration (normality) of each of both metals. The preparation of monometallic samples included one ion exchange step of NaMOR in an appropriate solution. Preparation of bimetallic samples included two steps of ion-exchange; labels of the bimetallic samples reflected the order of the cations incorporation during the ion exchange: AgFeMOR (first Ag^+, then Fe^{2+}) and FeAgMOR (first Fe^{2+}, then Ag^+).

3.2. Characterization Methods

Quantitative chemical analysis of the samples was carried out by Inductively Coupled Plasma-Optical Emission Spectroscopy (ICP-OES) method by means of a VARIAN VISTA-MPX CCD SIMULTANEOUS spectrometer (Varian Inc., Palo Alto, CA, USA). The samples were pretreated by degassing, followed by dissolution in a mixture of HNO_3 and HF at 40 °C overnight, and adding an H_3BO_3 solution, followed by further keeping at 40 °C for 5 h.

Textural properties were determined from nitrogen adsorption-desorption isotherms at −196 °C, recorded with a Micromeritics TriStar 3000 apparatus (Micromeritics Instruments Corp., Norcross, GA, USA). Prior to experiments, the samples were degassed at 300 °C in a vacuum for 5 h. The volume of the adsorbed N_2 was normalized to a standard temperature and pressure. The specific surface area (S_{BET}) of the samples was calculated by applying the Brunauer–Emmett–Teller (BET) method to the nitrogen adsorption data within the P/P_0 range of 0.005–0.250. The average pore diameter was calculated by applying the Barret–Joyner–Halenda (BJH) method to the adsorption and desorption branches of the N_2 isotherms. The cumulative pore volume was obtained from the isotherms at $P/P_0 = 0.99$.

Surface acidity was measured in a fixed bed continuous flow quartz micro-reactor, using approximately 50 mg of the sample over a temperature range of 100–550 °C at a heating rate ramp of 10 °C/min. The acidity of the samples was measured by the analysis of TCD-TPD (Thermal Conductivity Detector) with a Quantachrome Chem BET Pulsar TPD/TPD (Quantachrome, Boynton Beach, FL, USA). First, in order to remove moisture, the samples were pre-treated in He (99.99% purity, 120 mL/min, temperature range 100–550 °C, a heating rate of 10 °C/min). The sample was then left at 550 °C for 1 h and then cooled down to 100 °C. For the ammonia chemisorption probe, anhydrous ammonia with a purity of 99.98% Aldrich was used at a flow rate of 120 mL/min for 10 min at 100 °C. After that, adsorbed molecules were removed by applying a flow of He for 40 min.

Fe K-edge EXAFS spectra were measured in transmission mode at the Structural Materials Science end-station of the Kurchatov Synchrotron Radiation source [61]. To scan the energy, Si (111) channel-cut monochromator (Shubnikov Institute of Crystallography RAS, Moscow, Russia) was used. The X-ray beam intensities before and after the sample were measured with ionization chambers filled with air and Ar for Fe K-edge at atmospheric pressure. The primary processing of the XAFS spectra was carried out in terms of the IFEFFIT software package (version 0.9.26) [62,63]. Normalized EXAFS oscillations were k^3-weighted and analyzed in the 2÷12 $Å^{-1}$ k-range in the case of Fe K-edge spectra.

Fourier transformed infrared (FTIR) spectra of adsorbed NO were carried out in situ on an FTIR-66 spectrometer (Bruker, Manning Park Billerica, MA, USA) equipped with a cryogenic MCT (Mercury-Cadmium-Telluride) detector in transmittance mode with a resolution of 4 cm^{-1} over 64 total scans per spectrum. Samples in the form of thin self-supporting pellets (5–10 mg/cm^2) were directly treated at temperatures from room temperature to 500 °C and pressures from 10^{-2} to 760 Torr

in a quartz cell equipped with KBr windows, designed for room temperature studies in a controlled atmosphere. First, the samples were degassed under a dynamic vacuum of 10^{-3} mBar at 400 °C for 1 h, then cooled down to room temperature and then evacuated. The spectra were measured by dosing NO (70 mBar), and subsequently reducing the NO pressure by stepwise expansions in the vacuum line, followed by gradual opening to dynamic vacuum (final pressure 5.0×10^{-4} mBar). The spectra reported after normalization with respect to the intensity of the overtone framework modes at 1872 cm^{-1}.

Catalytic activity was measured in a fixed bed continuous flow quartz micro-reactor inside a vertical furnace, using 10 mg of the catalyst. Before the catalytic reaction, the catalysts were pretreated in a flow of an oxidant mixture (70 mL/min of 4.4 vol.% of O_2/N_2 balanced) at a heating rate of 5 °C/min from room temperature up to 550 °C. The catalytic activity of the samples was measured for NO reduction in the presence of CO, propene, and oxygen. Catalytic runs were performed within the temperature range of 25–500 °C at a rate of 10 °C/min. The reaction gas phase mixture consisted of NO (650 ppm), C_3H_6 (550 ppm), O_2 (2 vol.%), CO (0.4 vol.%) in N_2 balance and a total gas flow of 100 mL min^{-1}. This gas mixture emulated the vehicle exhaust gases from internal combustion engines. Inlet and outlet gas concentrations were measured in a ZAI gas analyzer. Data acquisition of NO concentration during the catalytic reaction was obtained continuously. Conversion of NO was calculated from the difference of the reactor inlet and outlet NO concentration, divided by the inlet NO concentration.

4. Conclusions

Monometallic and bimetallic Ag-Fe-based materials deposited on a mordenite carrier were prepared by the ion exchange method, applying different orders of metal deposition. It is shown that ion-exchange treatment very slightly changes the mordenite stoichiometry and textural properties. The second step of ion exchange may wash out some amount of the cations of the first step of ion-exchanged.

The results of Fe K-edge XANES oscillations showed that in FeMOR, both Fe^{3+} and Fe^{2+} were in a disordered state. In FeAgMOR, the prevailing state was Fe^{3+}, while in AgFeMOR, the iron states were intermediate, or mixed between FeMOR and FeAgMOR catalysts. The results of the Fe K-edge EXAFS study revealed the formation of a disordered state in which the first coordination sphere was asymmetric and was characterized by two different Fe-O distances. In FeAgMOR and AgFeMOR, the coordination of Fe-O was similar. Therefore, based on the EXAFS data, we may conclude that Fe is incorporated in FeAgMOR and AgFeMOR into the zeolite framework as Fe^{3+} instead of Al^{3+}, and in accordance with our knowledge, this is a new type of active center in the de-NO$_x$ reaction.

The catalytic activity results for the de-NO$_x$ reaction in the presence of CO/C_3H_6 showed that the most active samples were the Fe-containing ones. The mordenite carrier and the monometallic silver sample AgMOR did not show high activity in the studied reaction. The promoter effect of Ag on iron-containing catalysts took place at the high-temperature activity.

Based on the thermodynamic analysis and experimental data, a mechanism for the formation of active centers at two steps of ion-exchange synthesis with a different order of deposition of components was proposed and confirmed.

Author Contributions: P.S.-L.—samples synthesis and characterization, data curation, investigation, original draft preparation; Y.K.—conceptualization, data curation, investigation, original draft preparation; E.K.—methodology and investigation by EXAFS, review, and editing; R.K.C.—conceptualization, formal analysis, review, and editing; M.A.E.—methodology and investigation by TPD NH$_3$, review, and editing; G.B.—methodology and investigation by FTIR of adsorbed NO, review, and editing; Y.Z.—supervision, review, and editing; S.F.—funding acquisition, supervision, review, and editing; V.P.—formal analysis, investigation, supervision, original draft preparation; F.C.-R.—funding acquisition, supervision, review, and editing. All authors have read and agreed to the published version of the manuscript.

Conflicts of Interest: The authors declare no conflict of interest.

References

1. Li, J.; Wang, Y.; Qu, H. Dependence of Summertime Surface Ozone on NO_x and VOC Emissions over the United States: Peak Time and Value. *Geophys. Res. Lett.* **2019**, *46*, 3540–3550. [CrossRef]
2. Sillman, S. 11.11-Tropospheric Ozone and Photochemical Smog. In *Treatise on Geochemistry*, 2nd ed.; Holland, H.D., Turekian, K.K., Eds.; Elsevier: Amsterdam, The Netherlands, 2014; Volume 11, pp. 415–437.
3. De Richter, R.; Caillol, S. Fighting global warming: The potential of photocat alysis against CO_2, CH_4, N_2O, CFCs, tropospheric O_3, BC and other major contributors to climate change. *J. Photochem. Photobiol. C Photochem. Rev.* **2011**, *12*, 1–19. [CrossRef]
4. Johnson, T.V. Vehicular Emissions in Review. *SAE Int. J. Engines* **2012**, *5*, 216–234. [CrossRef]
5. Leinert, S.; Daly, H.; Hyde, B.; Gallachóir, B.Ó. Co-Benefits? Not always: Quantifying the negative effect of a CO_2-reducing car taxation policy on NO_x emissions. *Energy Policy* **2013**, *63*, 1151–1159. [CrossRef]
6. Oliva, P. Environmental Regulations and Corruption: Automobile Emissions in Mexico City. *J. Polit. Econ.* **2015**, *123*, 686–723. [CrossRef]
7. Environmental Protection Agency. Inventory of U.S. Greenhouse Gas Emissions and Sinks: 1990–2014. Available online: https://www.epa.gov/ghgemissions/inventory-us-greenhouse-gas-emissions-and-sinks-1990-2014 (accessed on 26 August 2020).
8. Ramos, A.; Muñoz, J.; Andrés, F.; Armas, O. NOx emissions from diesel light duty vehicle tested under NEDC and real-word driving conditions. *Transp. Res. Part D Transp. Environ.* **2018**, *63*, 37–48. [CrossRef]
9. Wei, H.; Liu, W.; Zhang, J.; Qin, Z. Effects of simulated acid rain on soil fauna community composition and their ecological niches. *Environ. Pollut.* **2017**, *220*, 460–468. [CrossRef]
10. Gurjar, B.R.; Jain, A.; Sharma, A.; Agarwal, A.; Gupta, P.; Nagpure, A.S.; Lelieveld, J. Human health risks in megacities due to air pollution. *Atmos. Environ.* **2010**, *44*, 4606–4613. [CrossRef]
11. Piumetti, M.; Bensaid, S.; Fino, D.; Russo, N. Catalysis in Diesel engine NO_x after treatment: A review. *Catal. Struct. React.* **2015**, *1*, 155–173. [CrossRef]
12. Xin, Y.; Li, Q.; Zhang, Z. Zeolitic Materials for DeNO$_x$ Selective Catalytic Reduction. *ChemCatChem* **2018**, *10*, 29–41. [CrossRef]
13. Mrad, R.; Aissat, A.; Cousin, R.; Courcot, D.; Siffert, S. Catalysts for NO_x selective catalytic reduction by hydrocarbons (HC-SCR). *Appl. Catal. A Gen.* **2015**, *504*, 542–548. [CrossRef]
14. Traa, Y.; Burger, B.; Weitkamp, J. Zeolite-based materials for the selective catalytic reduction of NO_x with hydrocarbons. *Microporous Mesoporous Mater.* **1999**, *30*, 3–41. [CrossRef]
15. Cant, N.W.; Liu, I.O.Y. Mechanism of the selective reduction of nitrogen oxides by hydrocarbons on zeolite catalysts. *Catal. Today* **2000**, *63*, 133–146. [CrossRef]
16. Bartolomeu, R.; Azambre, B.; Westermann, A.; Fernandes, A.; Bértolo, R.; Hamoud, H.I.; Henriques, C.; Da Costa, P.; Ribeiro, F. Investigation of the nature of silver species on different Ag-containing NO_x reduction catalysts: On the effect of the support. *Appl. Catal. B Environ.* **2014**, *150–151*, 204–217. [CrossRef]
17. Castellanos, I.; Marie, O. An operando FT-IR study of the NO_x SCR over Co-HFER and Fe-HFER using acetylene as a reducing agent. *Catal. Today* **2017**, *283*, 54–65. [CrossRef]
18. Čapek, L.; Kreibich, V.; Dedeček, J.; Grygar, T.; Wichterlová, B.; Sobalík, Z.; Martens, J.A.; Brosius, R.; Tokarová, V. Analysis of Fe species in zeolites by UV-VIS-NIR, IR spectra and voltammetry. Effect of preparation, Fe loading and zeolite type. *Microporous Mesoporous Mater.* **2005**, *80*, 279–289. [CrossRef]
19. Lee, K.; Kosaka, H.; Sato, S.; Yokoi, T.; Choi, B.; Kim, D. Effects of Cu loading and zeolite topology on the selective catalytic reduction with C_3H_6 over Cu/zeolite catalysts. *J. Ind. Eng. Chem.* **2019**, *72*, 73–86. [CrossRef]
20. Chen, H.Y.; Wang, X.; Sachtler, W.M.H. Reduction of NO_x over various Fe/zeolite catalysts. *Appl. Catal. A Gen.* **2000**, *194*, 159–168. [CrossRef]

21. Bin Lim, J.; Shin, J.; Ahn, N.H.; Heo, I.; Hong, S.B. Selective catalytic reduction of NO with CH_4 over cobalt-exchanged cage-based, small-pore zeolites with different framework structures. *Appl. Catal. B Environ.* **2020**, *267*, 118710.

22. Shibata, J.; Takada, Y.; Shichi, A.; Satokawa, S.; Satsuma, A.; Hattori, T. Influence of zeolite support on activity enhancement by addition of hydrogen for SCR of NO by propane over Ag-zeolites. *Appl. Catal. B Environ.* **2004**, *54*, 137–144. [CrossRef]

23. Hamoud, H.I.; Valtchev, V.; Daturi, M. Selective catalytic reduction of NO_x over Cu- and Fe-exchanged zeolites and their mechanical mixture. *Appl. Catal. B Environ.* **2019**, *250*, 419–428. [CrossRef]

24. Dorado, F.; De Lucas, A.; García, P.B.; Romero, A.; Valverde, J.L.; Asencio, I. SCR of NO by propene on monometallic (Co or Ni) and bimetallic (Co/Ag or Ni/Ag) mordenite-based catalysts. *Ind. Eng. Chem. Res.* **2005**, *44*, 8988–8996. [CrossRef]

25. Lee, K.; Choi, B.; Lee, C.; Oh, K. Effects of SiO_2/Al_2O_3 ratio, reaction atmosphere and metal additive on de-NO_x performance of HC-SCR over Cu-based ZSM-5. *J. Ind. Eng. Chem.* **2020**, *90*, 132–144. [CrossRef]

26. Serra, R.M.; Aspromonte, S.G.; Miró, E.E.; Boix, A.V. Hydrocarbon adsorption and NO_x-SCR on (Cs, Co) mordenite. *Appl. Catal. B Environ.* **2015**, *166–167*, 592–602. [CrossRef]

27. Cheng, X.; Su, D.; Wang, Z.; Ma, C.; Wang, M. Catalytic reduction of nitrogen oxide by carbon monoxide, methane and hydrogen over transition metals supported on BEA zeolites. *Int. J. Hydrog. Energy* **2018**, *43*, 21969–21981. [CrossRef]

28. Abu-Zied, B.M.; Schwieger, W.; Unger, A. Nitrous oxide decomposition over transition metal exchanged ZSM-5 zeolites prepared by the solid-state ion-exchange method. *Appl. Catal. B Environ.* **2008**, *84*, 277–288. [CrossRef]

29. Wang, J.; Zhao, H.; Haller, G.; Li, Y. Recent advances in the selective catalytic reduction of NO_x with NH_3 on Cu-Chabazite catalysts. *Appl. Catal. B Environ.* **2017**, *202*, 346–354. [CrossRef]

30. Kim, M.H.; Nam, I.; Kim, Y.G. Water tolerance of mordenite-type zeolite catalysts for selective reduction of nitric oxide by hydrocarbons. *Appl. Catal. B Environ.* **1997**, *12*, 125–145. [CrossRef]

31. Aspromonte, S.G.; Miró, E.E.; Boix, A.V. FTIR studies of butane, toluene and nitric oxide adsorption on Ag exchanged NaMordenite. *Adsorption* **2012**, *18*, 1–12. [CrossRef]

32. Gurin, V.S.; Petranovskii, V.P.; Hernandez, M.A.; Bogdanchikova, N.E.; Alexeenko, A.A. Silver and copper clusters and small particles stabilized within nanoporous silicate-based materials. *Mater. Sci. Eng. A* **2005**, *391*, 71–76. [CrossRef]

33. Shelyapina, M.G.; Gurgul, J.; Łątka, K.; Sánchez-López, P.; Bogdanov, D.; Kotolevich, Y.; Petranovskii, V.; Fuentes, S. Mechanism of formation of framework Fe^{3+} in bimetallic Ag-Fe mordenites—Effective catalytic centers for deNO$_x$ reaction. *Microporous Mesoporous Mater.* **2020**, *299*, 109841. [CrossRef]

34. Qian, W.; Su, Y.; Yang, X.; Yuan, M.; Deng, W.; Zhao, B. Experimental study on selective catalytic reduction of NO with propene over iron based catalysts supported on aluminum pillared clays. *J. Fuel Chem. Technol.* **2017**, *45*, 1499–1507. [CrossRef]

35. Zhang, X.; Su, Y.; Cheng, J.; Lin, R.; Wen, N.; Deng, W.; Zhou, H. Effect of Ag on deNO$_x$ performance of SCR-C_3H_6 over Fe/Al-PILC catalysts. *J. Fuel Chem. Technol.* **2019**, *47*, 1368–1378. [CrossRef]

36. Shi, J.; Zhang, Y.; Zhu, Y.; Chen, M.; Zhang, Z.; Shangguan, W. Efficient Fe-ZSM-5 catalyst with wide active temperature window for NH_3 selective catalytic reduction of NO: Synergistic effect of isolated Fe^{3+} and Fe_2O_3. *J. Catal.* **2019**, *378*, 17–27. [CrossRef]

37. Dzwigaj, S.; Janas, J.; Rojek, W.; Stievano, L.; Wagner, F.E.; Averseng, F.; Che, M. Effect of iron impurities on the catalytic activity of BEA, MOR and MFI zeolites in the SCR of NO by ethanol. *Appl. Catal. B Environ.* **2009**, *86*, 45–52. [CrossRef]

38. Sazama, P.; Pilar, R.; Mokrzycki, L.; Vondrova, A.; Kaucky, D.; Plsek, J.; Sklenak, S.; Stastny, P.; Klein, P. Remarkably enhanced density and specific activity of active sites in Al-rich Cu-, Fe- and Co-beta zeolites for selective catalytic reduction of NO_x. *Appl. Catal. B Environ.* **2016**, *189*, 65–74. [CrossRef]

39. Iwasaki, M.; Yamazaki, K.; Banno, K.; Shinjoh, H. Characterization of Fe/ZSM-5 DeNOx catalysts prepared by different methods: Relationships between active Fe sites and NH_3-SCR performance. *J. Catal.* **2008**, *260*, 205–216. [CrossRef]

40. Kumar, M.S.; Schwidder, M.; Grünert, W.; Bentrup, U.; Brückner, A. Selective reduction of NO with Fe-ZSM-5 catalysts of low Fe content: Part II. Assessing the function of different Fe sites by spectroscopic in situ studies. *J. Catal.* **2006**, *239*, 173–186.

41. Heijboer, W.M.; Battiston, A.A.; Knop-Gericke, A.; Hävecker, M.; Bluhm, H.; Weckhuysen, B.M.; Koningsberger, D.C.; de Groot, F.M.F. Redox behaviour of over-exchanged Fe/ZSM5 zeolites studied with in-situ soft X-ray absorption spectroscopy. *Phys. Chem. Chem. Phys.* **2003**, *5*, 4484. [CrossRef]

42. Boroń, P.; Chmielarz, L.; Gurgul, J.; Latka, K.; Gil, B.; Marszalek, B.; Dzwigaj, S. Influence of iron state and acidity of zeolites on the catalytic activity of FeHBEA, FeHZSM-5 and FeHMOR in SCR of NO with NH_3 and N_2O decomposition. *Microporous Mesoporous Mater.* **2015**, *203*, 73–85. [CrossRef]

43. Shwan, S.; Jansson, J.; Olsson, L.; Skoglundh, M. Effect of post-synthesis hydrogen-treatment on the nature of iron species in Fe-BEA as NH_3-SCR catalyst. *Catal. Sci. Technol.* **2014**, *4*, 2932. [CrossRef]

44. Bartolomeu, R.; Mendes, N.; Fernandes, A. NO_x SCR with decane using Ag-MFI catalysts: On the effect of silver content and co-cation presence. *Catal. Sci. Technol.* **2016**, *6*, 3038–3048. [CrossRef]

45. Satsuma, A.; Shibata, J.; Shimizu, K.I.; Hattori, T. Ag clusters as active species for HC-SCR over Ag-zeolites. *Catal. Surv. Asia* **2005**, *9*, 75–85. [CrossRef]

46. Shimizu, K.; Sugino, K.; Kato, K.; Yokota, S.; Okumura, K. Reaction Mechanism of H_2-Promoted Selective Catalytic Reduction of NO with C_3H_8 over Ag–MFI Zeolite. *J. Phys. Chem. C* **2007**, *111*, 6481–6487. [CrossRef]

47. Shimizu, K.I.; Satsuma, A. Selective catalytic reduction of NO over supported silver catalysts—Practical and mechanistic aspects. *Phys. Chem. Chem. Phys.* **2006**, *8*, 2677–2695. [CrossRef]

48. More, P.M.; Nguyen, D.L.; Granger, P.; Dujardin, C.; Dongare, M.K.; Umbarkar, S.B. Activation by pretreatment of Ag-Au/Al$_2$O$_3$ bimetallic catalyst to improve low temperature HC-SCR of NO_x for lean burn engine exhaust. *Appl. Catal. B Environ.* **2015**, *174–175*, 145–156. [CrossRef]

49. More, P.M.; Nguyen, D.L.; Dongare, M.K.; Umbarkar, S.B.; Nuns, N.; Girardon, J.-S.; Dujardin, C.; Lancelot, C.; Mamede, A.S.; Granger, P. Rational preparation of Ag and Au bimetallic catalysts for the hydrocarbon-SCR of NO_x: Sequential deposition vs. coprecipitation method. *Appl. Catal. B Environ.* **2015**, *162*, 11–20. [CrossRef]

50. Sánchez-López, P.; Kotolevich, Y.; Miridonov, S.; Chávez-Rivas, F.; Fuentes, S.; Petranovskii, V. Bimetallic AgFe Systems on Mordenite: Effect of Cation Deposition Order in the NO Reduction with C_3H_6/CO. *Catalysts* **2019**, *9*, 58. [CrossRef]

51. Motsi, T.; Rowson, N.A.; Simmons, M.J.H. Adsorption of heavy metals from acid mine drainage by natural zeolite. *Int. J. Miner. Process.* **2009**, *92*, 42–48. [CrossRef]

52. Wang, X.S.; Huang, J.; Hu, H.Q.; Wang, J.; Qin, Y. Determination of kinetic and equilibrium parameters of the batch adsorption of Ni (II) from aqueous solutions by Na-mordenite. *J. Hazard. Mater.* **2007**, *142*, 468–476. [CrossRef]

53. Lee, S.H.; Jo, H.Y.; Yun, S.T.; Lee, Y.J. Evaluation of factors affecting performance of a zeolitic rock barrier to remove zinc from water. *J. Hazard. Mater.* **2010**, *175*, 224–234. [CrossRef] [PubMed]

54. Trgo, M.; Perić, J. Interaction of the zeolitic tuff with Zn containing simulated pollutant solutions. *J. Colloid Interface Sci.* **2003**, *260*, 166–175. [CrossRef]

55. Nakamura, H.; Okumura, M.; Machida, M. First-Principles Calculation Study of Mechanism of Cation Adsorption Selectivity of Zeolites: A Guideline for Effective Removal of Radioactive Cesium. *J. Phys. Soc. Jpn.* **2013**, *82*, 023801. [CrossRef]

56. Seliman, A.F.; Borai, E.H. Utilization of natural chabazite and mordenite as a reactive barrier for immobilization of hazardous heavy metals. *Environ. Sci. Pollut. Res.* **2011**, *18*, 1098–1107. [CrossRef]

57. Smith, D.W. Ionic Hydration Enthalpies. *J. Chem. Educ.* **1977**, *54*, 540–542. [CrossRef]

58. Luo, Y.R. *Comprehensive Handbook of Chemical Bond. Energies*, 1st ed.; CRC Press: Boca Raton, FL, USA, 2007.

59. Berlier, G.; Lamberti, C.; Rivallan, M.; Mul, G. Characterization of Fe sites in Fe-zeolites by FTIR spectroscopy of adsorbed NO: Are the spectra obtained in static vacuum and dynamic flow set-ups comparable. *Phys. Chem. Chem. Phys.* **2010**, *12*, 358–364. [CrossRef]

60. Brandenberger, S.; Kröcher, O.; Tissler, A.; Althoff, R. The State of the Art in Selective Catalytic Reduction of NO_x by Ammonia Using Metal-Exchanged Zeolite Catalysts. *Catal. Rev.* **2008**, *50*, 492–531. [CrossRef]

61. Trofimova, N.N.; Veligzhanin, A.A.; Murzin, V.Y.; Chernyshov, A.A.; Khramov, E.V.; Zabluda, V.N.; Edel'man, I.S.; Slovokhotov, Y.L.; Zubavichus, Y.V. Structural diagnostics of functional nanomaterials with the use of X-ray synchrotron radiation. *Nanotechnol. Russ.* **2013**, *8*, 396–401. [CrossRef]

62. Ravel, B.; Newville, M. Athena, Artemis, Hephaestus: Data analysis for X-ray absorption spectroscopy using IFEFFIT. *J. Synchrotron Radiat.* **2005**, *12*, 537–541. [CrossRef]

63. Newville, M. IFEFFIT: Interactive XAFS analysis and FEFF fitting. *J. Synchrotron Radiat.* **2001**, *8*, 322–324. [CrossRef]